PHYSICAL REVIEW E, VOLUME 64, 055202(R)

Spatiotemporal patterns in CO oxidation on Pt(110): The role of nonlinear diffusion

J. Verdasca,* P. Borckmans, and G. Dewel
Service de Chimie-Physique, Code Postal 231, Université Libre de Bruxelles, 1050 Bruxelles, Belgium
(Received 22 August 2000; revised manuscript received 5 July 2001; published 15 October 2001)

Standing-wave patterns observed in the $CO+O_2$ reaction on Pt(110) are described by a model that explicitly takes into account the coupling between the transport of adsorbed CO and the adsorbate-induced structural transformation of the substrate. We show that synchronization of the surface is achieved through nucleation and growth processes even in the absence of gas-phase coupling.

DOI: 10.1103/PhysRevE.64.055202 PACS number(s): 82.65.+r, 68.35.Bs, 68.43.Mn, 81.65.Mq

A rich variety of spatiotemporal patterns has been observed during the catalytic CO oxidation on Pt(110) surfaces under isothermal and ultrahigh vacuum conditions. Modern surface imaging techniques with high spatial resolution have provided real time pictures of propagating fronts, spiral waves, target patterns, standing waves, and chemical turbulence [1–4]. Before these spatial features could be resolved, work function measurements had already revealed that the reaction rate may become oscillatory and even chaotic [5,6]. The mechanism driving the oscillations is an adsorbate-induced structural phase transition (SPT) of the surface: clean Pt(110) surfaces are reconstructed presenting a 1×2 missing-row structure; this reconstruction is reversibly lifted by a critical coverage of CO, which causes the surface to revert to the bulk termination — a 1×1 structure [7]. The dependence of the oxygen adsorption probability on these structural modifications induces then the periodic switching of the surface between states of high and low catalytic activity.

A model developed by Krischer *et al.* [6] — and coined the KEE model — correctly describes the domain of oscillations in the plane defined by the partial pressures of CO and O_2, respectively p_{CO} and p_{O_2}, reaching semiquantitative agreement with observed oscillation profiles. However, the KEE model presents a chaotic attractor only for unrealistic parameter values, reinforcing the belief that a realistic model would have to take spatial variations into account. A first attempt to include spatial effects [8], by introducing a Fickian diffusion term for the mobile adspecies CO_{ad}, failed in producing robust spatiotemporal patterns. Facing this failure, global coupling through the gas phase has since been invoked to explain the occurrence of synchronized patterns [4,3,9].

The notion that global coupling is an essential ingredient for coherent spatiotemporal patterns to arise in this system has recently been challenged by Monte Carlo (MC) simulations [10]. These studies also stressed the crucial role played by nucleation and growth of phase domains in the establishment of synchronized behavior. However, MC simulations cannot predict the symmetry of the patterns because the number of particles involved is too small. Hence, for the moment, MC results cannot provide a basis for the interpretation of experimental data. Thus, in this Rapid Communication we go back to a macroscopic description of the $CO+O_2$ reaction on Pt(110), though we abandon the traditional ''reaction-diffusion'' scenario with Fickian terms in favor of generalized mass balance equations that consistently incorporate the coupling between mass transport in the adlayer and the SPT. We will see that the model developed here allows for a more detailed analysis of the observed patterns than can currently be achieved by other methods.

An adsorbate-induced surface phase transition is a complex phenomenon. We consider a simple mean-field model based on the lattice gas [11]. The corresponding local free-energy density can be represented as the sum of three contributions: $f=f_{ad}+f_s+f_{int}$. The free-energy density of the adsorbed layer is that of a ternary mixture composed of adsorbed CO molecules and O atoms *plus* the unoccupied adsorption sites:

$$f_{ad}=-E_{CO}^{1\times2}\theta_{CO}-E_{O}^{1\times2}\theta_{O}+RT[\theta_{CO}\ln\theta_{CO}+\theta_{O}\ln\theta_{O}+(1-\theta_{CO}-\theta_{O})\ln(1-\theta_{CO}-\theta_{O})], \quad (1)$$

where $E_{CO}^{1\times2}(E_{O}^{1\times2})$ is the CO (oxygen) adsorption energy in the reconstructed phase, θ_{CO} and θ_{O} being the surface coverages of each reactant species. The second term is the free energy of the clean surface,

$$f_s=\Delta E\kappa+RT[\kappa\ln\kappa+(1-\kappa)\ln(1-\kappa)], \quad (2)$$

ΔE being the energy difference between the clean 1×1 and 1×2 surfaces, and κ the fraction of the surface in the 1×1 configuration. In Eq. (1) we have neglected the contribution of lateral interactions between adsorbed molecules. The last term $f_{int}=-\alpha\theta_{CO}\kappa$ describes the interaction between surface atoms and adsorbed molecules: α is the difference in the heats of adsorption of CO between the two surface phases that provides the driving force for surface transformation. The free-energy functional describing large scale inhomogeneities is obtained by adding to $f(\theta_{CO},\theta_{O},\kappa)$ a contribution due to coverage gradients of the mobile adspecies (CO) up to first order, then integrating over the whole surface area:

$$\mathcal{F}\{\theta_{CO},\theta_{O},\kappa\}=\int d\mathbf{r}\left[f(\theta_{CO},\theta_{O},\kappa)+\frac{\gamma}{2}(\nabla\theta_{CO})^2\right], \quad (3)$$

*Present address: Centro de Física da Matéria Condensada, Av. Prof. Gama Pinto, 2, P-1649-003 Lisboa, Portugal.

where $\gamma = RT\xi_0^2$, ξ_0 being a phenomenological characteristic length.

The mass balance equations for the adsorbed CO and O then take the following form:

$$\frac{\partial \theta_{\mathrm{CO}}}{\partial t} = p_{\mathrm{CO}} s_{\mathrm{CO}} k_{\mathrm{CO}} (1 - \theta_{\mathrm{CO}}^r) - k_d \theta_{\mathrm{CO}} - k_r \theta_{\mathrm{CO}} \theta_{\mathrm{O}} - \boldsymbol{\nabla} \cdot \mathbf{J}_{\mathrm{CO}}, \tag{4}$$

$$\frac{\partial \theta_{\mathrm{O}}}{\partial t} = p_{\mathrm{O}_2} s_{\mathrm{O}} k_{\mathrm{O}} (1 - \theta_{\mathrm{CO}} - \theta_{\mathrm{O}})^2 - k_r \theta_{\mathrm{CO}} \theta_{\mathrm{O}}, \tag{5}$$

where $k_{\mathrm{CO}}, s_{\mathrm{CO}}$, and $k_{\mathrm{O}}, s_{\mathrm{O}}$ are the rate constants for adsorption and the sticking coefficients of, respectively, carbon monoxide and oxygen; k_d and k_r are the rate constants for CO desorption and chemical reaction.

The kinetic source terms have been established before [6]: reaction takes place through the Langmuir-Hinshelwood mechanism; oxygen adsorption is dissociative — hence quadratic in the number of empty sites — and inhibited by preadsorbed CO, while adsorption of CO takes place through a precursor state and is not prevented by adsorbed oxygen. The effect of the precursor adsorption is accounted for by the exponent $r > 1$ in the rhs of Eq. (4) [12]. Besides, O desorption can be neglected below 550 K.

The diffusive current of adsorbed CO, $\mathbf{J}_{\mathrm{CO}}$, is driven by the gradient of the chemical potential μ_{CO}:

$$\mathbf{J}_{\mathrm{CO}} = -M \nabla \mu_{\mathrm{CO}} = -M \boldsymbol{\nabla} \left\{ \frac{\delta \mathcal{F}}{\delta \theta_{\mathrm{CO}}} \right\}, \tag{6}$$

M being the surface mobility, taken as a constant. Moreover, in the temperature range of the experiments, oxygen is virtually immobile on the surface, which explains why there are no transport terms in Eq. (5).

Oscillations are not predicted by Eqs. (4) and (5) alone; the structural transformation of the substrate must be taken into account also. The coupling to a third equation ruling the dynamics of the SPT arises through the dependence of the oxygen sticking coefficient on the state of the surface, by putting $s_{\mathrm{O}}(\kappa) = s_{\mathrm{O}}^{1\times 1}\kappa + s_{\mathrm{O}}^{1\times 2}(1-\kappa)$, where $s_{\mathrm{O}}^{1\times 1}$ and $s_{\mathrm{O}}^{1\times 2}$ are, respectively, the sticking coefficients on the 1×1 and 1×2 surfaces [6]. Here, we use the estimate $S_{\mathrm{O}}^{1\times 1}/S_{\mathrm{O}}^{1\times 2} = 2$ [13], which compares well to experiment [14]. Such a difference in reactivity between the two surface phases introduces a negative feedback loop into the system that results in oscillations.

An important alternative aspect of our approach is that from the same functional (3) both the flux of CO (6) and the evolution equation for $\kappa(\mathbf{r},t)$ can be consistently derived. We do so by observing that during the adsorbate-induced SPT the surface is able to entirely switch from one atomic arrangement to another without constraint, namely in the form of a conservation law. In other words, $\kappa(\mathbf{r},t)$ is a nonconserved order parameter. Hence [15],

$$\frac{\partial \kappa}{\partial t} = -L \frac{\delta \mathcal{F}\{\theta_{\mathrm{CO}}, \theta_{\mathrm{O}}, \kappa\}}{\delta \kappa}, \tag{7}$$

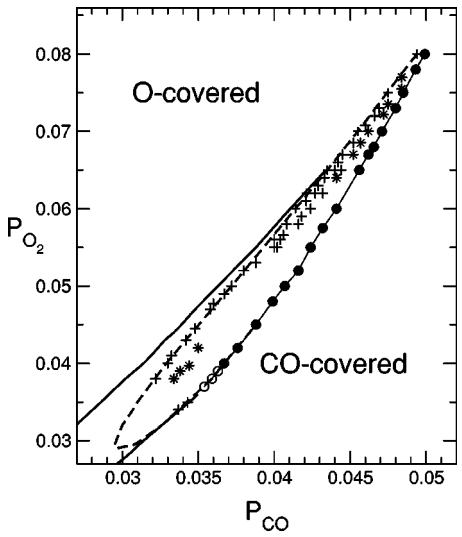

FIG. 1. The domain of complex spatiotemporal behavior in 1D systems of 256 cells. Parameters are $\Delta\overline{E} = 5.0$, $\overline{\alpha} = 18.0$, $\overline{M} = 5.0 \times 10^{-5}$, $d = 0.03$, and $\overline{L} = 5.0 \times 10^{-4}$. The filled circles represent uniform relaxation-type oscillations with very long periods. The crosses (+) are SW solutions (all of them 2:1 resonances) and the stars (*), turbulent patterns. Empty circles correspond to SW patterns associated with nonharmonic temporal profiles, obtained near the codimension-2 Hopf-SNIPER point. Finally, the solid lines connect points where the Turing bifurcation takes place. Structures arising between them and below the dashed line are stationary.

where L is a constant fixing the time scale of the SPT.

Inserting the explicit expressions for $\mathbf{J}_{\mathrm{CO}}$ and $\delta\mathcal{F}/\delta\kappa$, respectively, into Eqs. (4) and (7), one obtains, upon joining Eq. (5), a set of three coupled nonlinear pde's for the field variables $\theta_{\mathrm{CO}}(\mathbf{r},t), \theta_{\mathrm{O}}(\mathbf{r},t)$, and $\kappa(\mathbf{r},t)$. These can be put in the following form:

$$\frac{\partial \theta_{\mathrm{CO}}}{\partial \tau} = P_{\mathrm{CO}}(1 - \theta_{\mathrm{CO}}{}^3) - d\,\theta_{\mathrm{CO}} - \theta_{\mathrm{CO}}\theta_{\mathrm{O}} + \overline{M} \nabla_X^2 \left[\ln\left(\frac{\theta_{\mathrm{CO}}}{1 - \theta_{\mathrm{CO}} - \theta_{\mathrm{O}}} \right) - \overline{\alpha}\kappa - \nabla_X^2 \theta_{\mathrm{CO}} \right], \tag{8}$$

$$\frac{\partial \theta_{\mathrm{O}}}{\partial \tau} = P_{\mathrm{O}_2}(1+\kappa)(1 - \theta_{\mathrm{CO}} - \theta_{\mathrm{O}})^2 - \theta_{\mathrm{CO}}\theta_{\mathrm{O}} \tag{9}$$

$$\frac{\partial \kappa}{\partial \tau} = -\overline{L} \left[\Delta\overline{E} + \ln\left(\frac{\kappa}{1-\kappa} \right) - \overline{\alpha}\theta_{\mathrm{CO}} \right], \tag{10}$$

where we have defined adimensional time $\tau = k_r t$ and space $X = \xi_0^{-1} x$ variables, as well as $P_{\mathrm{CO}} = p_{\mathrm{CO}} s_{\mathrm{CO}} k_{\mathrm{CO}}/k_r$ and $P_{\mathrm{O}_2} = p_{\mathrm{O}_2} k_{\mathrm{O}_2} S_{\mathrm{O}}^{1\times 2}/k_r$. We also have $d = k_d/k_r$, $\overline{M} = RTM/k_r\xi_0^2$, and $\overline{L} = RTL/k_r$; $\overline{\alpha} = \alpha/RT$ and $\Delta\overline{E} = \Delta E/RT$ are the adimensional energetic parameters. We take $r = 3$ in Eq. (4), the nearest integer smaller than the estimated value [6].

In the absence of spatial terms, our model exhibits homogeneous oscillations in a narrow region of the phase diagram (Fig. 1) connecting two homogeneous steady states denoted,

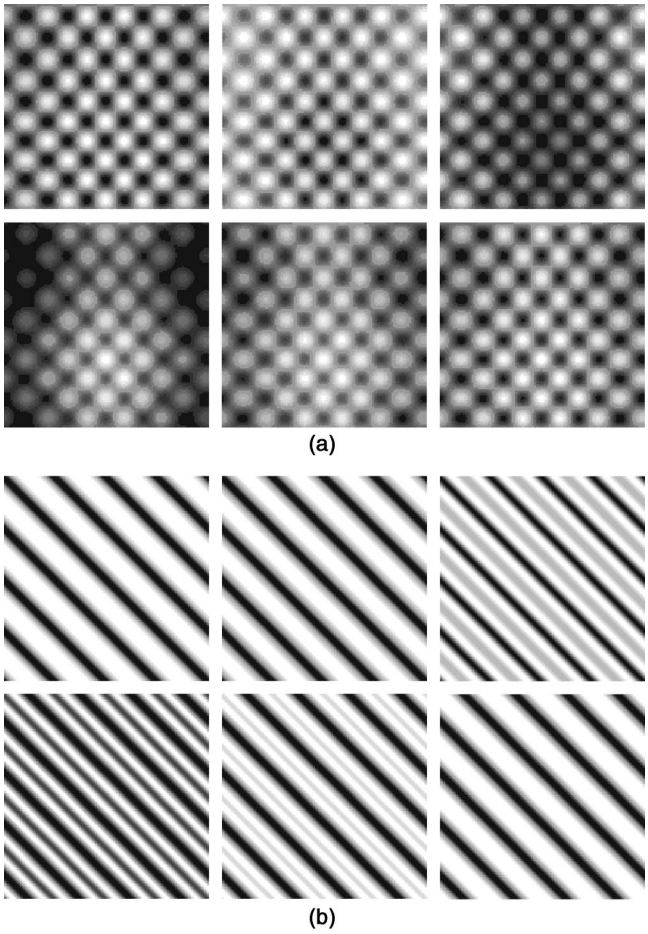

FIG. 2. Evolution of a SW pattern during half a period. (a) Oscillating squares. Parameter values are $P_{CO}=0.0728$, $P_{O_2}=0.11$, $\Delta\overline{E}=5.0$, $\overline{\alpha}=18.0$, $d=0.05$, $\overline{M}=5.0\times10^{-5}$, and $\overline{L}=5.0\times10^{-4}$. From left to right, top to bottom, the time between two consecutive images is respectively $\tau=100$, 250, 150, 150, and 100. (b) SW pattern with stripe symmetry at $P_{CO}=0.0353$, $P_{O_2}=0.037$, $d=0.03$, and $\overline{M}=2.5\times10^{-5}$; $\Delta\overline{E}$, $\overline{\alpha}$, and $\overline{L}$ are the same as in (a). Time interval between successive images: $\tau=400$, 200, 100, 200, and 200. Periodic boundary conditions in both cases.

respectively, O-covered (low p_{CO}) and CO-covered (high p_{CO}). As in the case of the KEE model [6], the oscillatory domain is bounded from the left by a (dashed) line of Hopf bifurcations that starts right at the cusp at the top, reaches a turning point in the lower part of the diagram, and rises again until it meets a line of saddle-node infinite period (SNIPER) bifurcations.

Stable homogeneous oscillations still exist in the presence of the spatial coupling described in Eq. (8); but their domain of stability is reduced. Next to the uniform oscillations, one finds solutions also breaking spatial symmetry. At sufficient high values of P_{O_2}, an increase in P_{CO} leads to the destabilization of these solutions before the SNIPER threshold. This instability gives rise to a subharmonic standing-wave (SW) pattern. In reality it consists rather in the superposition of an homogeneous background oscillation and a SW with twice the period of the spatially averaged fields, but we shall call it simply a standing-wave for clarity purposes.

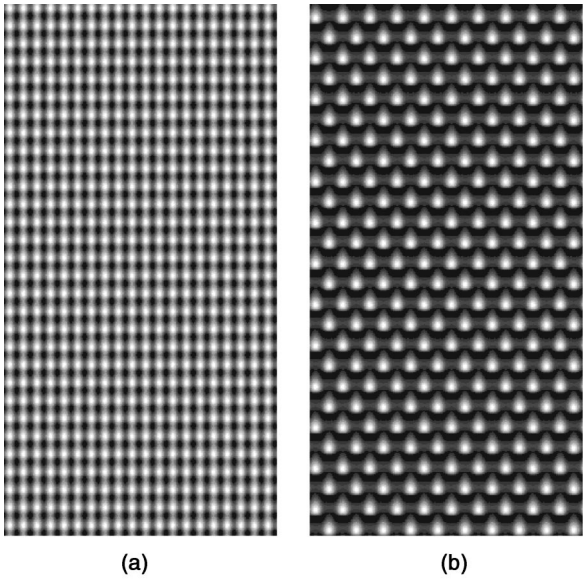

FIG. 3. Spatiotemporal charts showing 1:1 and 2:1 resonances as the control parameter P_{CO} is varied at fixed $P_{O_2}=0.06$, $\Delta\overline{E}=5.0$, $\overline{\alpha}=18.0$ and $\overline{M}=5.0\times10^{-5}$. (a) 1:1 resonance at $P_{CO}=0.0413$. (b) 2:1 pattern at $P_{CO}=0.04135$. Periodic BC. The integration time, $\tau=20000.$, is the same for both charts (time runs downwards).

This self-resonant behavior results from a periodic nucleation and growth of phase separated domains. As the system is periodically driven inside and out the thermodynamically unstable region, there is an outbreak of phase separated domains that subsequently synchronizes by the coupling effect of the homogeneous mode. If during one period of oscillation, the system's variables only assume such unstable values for a short while, phase separated domains will not have enough time to develop and the system will remain spatially uniform. This occurs for the homogeneous relaxation-type oscillations that exist near the SNIPER bifurcation line. As the oscillation profiles get smoother, the part of the cycle spent inside the unstable region increases and may become comparable to the characteristic time of phase separation, ultimately leading to a resonant spatiotemporal pattern. Hence, relaxation oscillations with large periods are homogeneous, while SW patterns usually appear associated with fast, quasiharmonic oscillations. The above picture is consistent with theory and observations of periodic spinodal decomposition [16].

In two dimensions (2D), according to the value of the desorption rate parameter d, the SW patterns exhibit either stripe or square symmetry. The time evolution of these patterns during one half period is shown in Fig. (2). Note that in the last frame of each sequence the regions where θ_O is lower (bright regions) are displaced by one half wavelength with respect to the first frame. The second half period merely repeats the sequence shown in the figure only at shifted locations, until the pattern in the first frame is recovered. In Fig. 2(b) we can see the emergence of a dark O-rich front that splits the CO-covered band in two creating a pair of

stripes that move apart. These stripes then collide and merge one wavelength away, only to be separated again later by a new splitting front growing from within, so that the initial pattern is repeated. The reverse case where a bright CO front bursts from the middle of a dark O-rich band was also observed. Both scenarios are in good agreement with experimental observations [4].

Upon a change in the partial pressures, the SW patterns may undergo a phase instability ultimately leading to a form of chemical turbulence characterized by a proliferation of spatiotemporal defects. Standing-wave fragments then coexist on the surface with oscillatory domains of irregular shapes and rapidly moving wave fronts. This scenario resembles that proposed recently by Argentina *et al.* [17], who have shown that a limit cycle is generically unstable with respect to inhomogeneous perturbations, on the approach to an homoclinic bifurcation, the instability being either a period doubling bifurcation with finite wave number or a phase instability. In 2D, the need for simultaneous conservation of the frequencies and wave vectors precludes the occurrence of quadratic terms in the amplitude equations describing SW patterns near the subharmonic instability [18]. Standing waves characterized by three resonant wave vectors, $\mathbf{k}_1+\mathbf{k}_2+\mathbf{k}_3=0$ cannot occur. Thus, in agreement with experiments [1], oscillating rhombs are obtained and not hexagons.

The present model predicts the existence of stationary (Turing) patterns in a band, shown in Fig. (1), that is the continuation of the oscillatory domain for decreasing values of P_{CO} and P_{O_2}. On the low P_{CO} side, the interaction between Turing and Hopf bifurcations gives rise in a narrow strip to several types of mixed-mode states that have been predicted to appear near codimension-two points where these two instabilities coincide [19]. As an example, the space-time plot of a Turing-Hopf mixed mode obtained in one-dimensional (1D) simulations is shown in Fig. 3(a); it corresponds to a stationary structure that oscillates with the Hopf critical frequency. A small increase in P_{CO} beyond the Hopf threshold (in the direction of the SNIPER line) renders the mixed mode unstable to the subharmonic instability [Fig. 3(b)]. The latter becomes phase unstable when P_{CO} is further increased leading to spatiotemporal chaos.

We have presented a model for the oscillating CO oxidation on Pt(110) that accounts for the strong dependence of CO diffusion on the dynamics of the structural phase transition of the substrate, through a nonlinear transport term. This ''up-hill'' diffusion plays a central role in pattern formation, with patches of CO_{od}-1×1 acting as traps for CO molecules migrating on adjacent reconstructed domains. For realistic values of the energetic parameters ΔE and α, the model succeeded in reproducing the main qualitative features of the observed patterns, without appealing to global coupling. The pattern symmetries, the subharmonic character of the oscillations, and even fine details of oscillating stripe patterns were all found to match experimental observations in an unprecedented way. The approach may be readily applied to other cases — like, for instance, electrocatalytic systems [20] — where a phase transition and chemical reactions concur to the formation of nonequilibrium patterns.

P.B. and G.D. acknowledge financial support from the FNRS (Belgium). J.V. received support from JNICT (Portugal) under the program PRAXIS XXI (BD-5977/95).

[1] S. Jakubith *et al.*, Phys. Rev. Lett. **65**, 3013 (1990).
[2] M. Bär *et al.*, Phys. Rev. Lett. **74**, 1246 (1995); S. Nettesheim *et al.*, J. Chem. Phys. **98**, 9977 (1993); H.H. Rotermund *et al.*, Phys. Rev. Lett. **66**, 3083 (1991).
[3] K.C. Rose *et al.*, Phys. Rev. Lett. **76**, 3582 (1996).
[4] A. von Oertzen *et al.*, J. Phys. Chem. B **104**, 3155 (2000).
[5] M. Eiswirth, K. Krischer, and G. Ertl, Surf. Sci. **202**, 565 (1988).
[6] K. Krischer, M. Eiswirth, and G. Ertl, J. Chem. Phys. **96**, 9161 (1992).
[7] T. Gritsch *et al.* Phys. Rev. Lett. **63**, 1086 (1989).
[8] H. Levine and X. Zou, Phys. Rev. Lett. **69**, 204 (1992).
[9] R. Imbihl and G. Ertl, Chem. Rev. **95**, 697 (1995); M. Falcke and H. Engel, Phys. Rev. E **50**, 1353 (1994); F. Mertens, R. Imbihl, and A. Mikhailov, J. Chem. Phys. **101**, 9903 (1994).
[10] O. Kortlüke, V.N. Kuzovkov, and W. von Niessen, Phys. Rev. Lett. **83**, 3089 (1999); V.P. Zhdanov, Surf. Sci. **426**, 345 (1999).
[11] V.P. Zhdanov, Surf. Sci. Lett. **164**, L807 (1985).
[12] R.P.H. Gasser and E.B. Schmidt, Chem. Phys. Lett. **1**, 457 (1967).
[13] In a context where the $[1\bar{1}0]$ atomic rows on Pt(110) are identified as the active sites for initial adsorption and dissociation of molecular oxygen, this value must be considered as a theoretical upper limit.
[14] N. Freyer *et al.*, Surf. Sci. **166**, 206 (1986).
[15] P.C. Hohenberg and B.I. Halperin, Rev. Mod. Phys. **49**, 435 (1977).
[16] A. Onuki, Phys. Rev. Lett. **48**, 753 (1982).
[17] M. Argentina, P. Coullet, and E. Risler, Phys. Rev. Lett. **86**, 807 (2001).
[18] L.M. Pismen, Dyn. Stab. Sys. **1**, 97 (1986).
[19] A. De Wit *et al.*, Phys. Rev. E **54**, 261 (1996).
[20] Y. Li *et al.*, Science **291**, 2395 (2001).